THE JOURNAL OF PHYSICAL CHEMISTRY B

ARTICLE

pubs.acs.org/JPCB

Direct Hydride Shift Mechanism and Stereoselectivity of $P450_{nor}$ Confirmed by QM/MM Calculations

Balázs Krámos,[†] Dóra K. Menyhárd,[‡] and Julianna Oláh*[,§]

[†]Department of Inorganic and Analytical Chemistry, Budapest University of Technology and Economics, Szent Gellért tér 4, H-1521 Budapest, Hungary

[‡]Laboratory of Structural Chemistry and Biology, Institute of Chemistry, Eötvös Loránd University, Pázmány Péter sétány 1/A, Budapest H-1117, Hungary

[§]Materials Structure and Modeling Research Group of the Hungarian Academy of Sciences, Budapest University of Technology and Economics, P.O. Box 91, H-1521 Budapest, Hungary

Supporting Information

ABSTRACT: Nitric oxide reductase ($P450_{nor}$) found in *Fusarium oxysporum* catalyzes the reduction of nitric oxide to N_2O in a multistep process. The reducing agent, NADH, is bound in the distal pocket of the enzyme, and direct hydride transfer occurs from NADH to the nitric oxide bound heme enzyme, forming intermediate *I*. Here we studied the possibility of hydride transfer from NADH to both the nitrogen and oxygen of the heme-bound nitric oxide, using quantum chemical and combined quantum mechanics/molecular mechanics (QM/MM) calculations, on two different protein models, representing both possible stereochemistries, a *syn*- and an *anti*-NADH arrangement. All calculations clearly favor hydride transfer to the nitrogen of nitric oxide, and the QM-only barrier and kinetic isotope effects are good agreement with the experimental values of intermediate *I* formation. We obtained higher barriers in the QM/MM calculations for both pathways, but hydride transfer to the nitrogen of nitric oxide is still clearly favored. The barriers obtained for the *syn*, Pro-R conformation of NADH are lower and show significantly less variation than the barriers obtained in the case of *anti* conformation. The effect of basis set and wide range of functionals on the obtained results are also discussed.

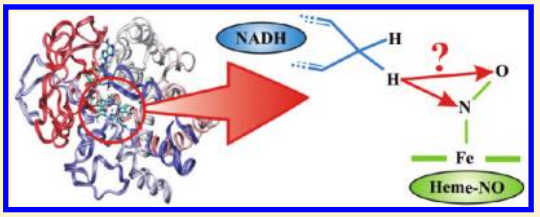

1. INTRODUCTION

The superfamily of cytochrome P450 enzymes (P450s) consists of proteins with a cysteine-ligated heme group in their active site. Most P450s catalyze a variety of oxidation reactions (e.g., hydroxilations, epoxidations, demethylation)[1] in the presence of redox partners that supply the two electrons needed in their catalytic cycle,[2] in a coupled and stepwise manner. P450 nitric oxide reductases form a distinct group of P450 enzymes: they catalyze the reduction of NO to N_2O, deriving the necessary electrons directly from NADPH or NADH, without the need for a redox-partner. An example of P450 nitric oxide reductases is found in the fungus *Fusarium oxysporum* (in this study under $P450_{nor}$ we mean the enzyme found in this species), which uses it, in the absence of O_2, to complete the denitrification process and gain energy for its vital cellular processes. The produced N_2O gas has a 300 times larger greenhouse effect than carbon dioxide,[3] so in chemically fertilized nitrate abundant area, the contribution of *Fusarium oxysporium* to producing greenhouse gases should be taken into account.[4]

The binding of nitric oxide itself to heme compounds and hemeproteins has been the subject of many experimental and computational studies. NO is known to bind strongly both to ferrous and ferric hemes. Furthermore, nitric oxide plays an important role in mammals: e.g., as a neurotransmitter, or as part of the immune response against pathogens.[5] However, several pathogens have developed a defense mechanism against the immune system-derived nitric oxide. One of these species, *Histoplasma capsulatum*, a fungal respiratory pathogen, uses the Nor1p enzyme to reduce nitric oxide, and avoid the nitrosative damage.[6] This enzyme has very high sequence and structural similarity (61% identity,79% similarity)[6] with $P450_{nor}$, suggesting a possibly similar mechanism for nitric oxide reduction. Understanding the catalytic mechanism of $P450_{nor}$ could be helpful in developing medication against *Histoplasma capsulatum* and similar pathogens.

$P450_{nor}$ of *Fusarium oxysporum* is a soluble protein found in the cytosol. It is selective for binding NADH: it cannot use NADPH as a reducing agent.[7] The NADH-binding pocket of $P450_{nor}$ is unlike the typical NADH binding pocket (Rossmanfold) found in other enzymes.[8] The catalytic cycle of $P450_{nor}$ consists of three main steps:

$$Fe(III)P450_{nor} + NO = (Fe(III)P450_{nor})NO$$

$$(Fe(III)P450_{nor})NO + NADH = I + NAD^+$$

$$I + NO + H^+ = Fe(III)P450_{nor} + N_2O + H_2O$$

Received: August 22, 2011
Revised: November 21, 2011
Published: December 10, 2011

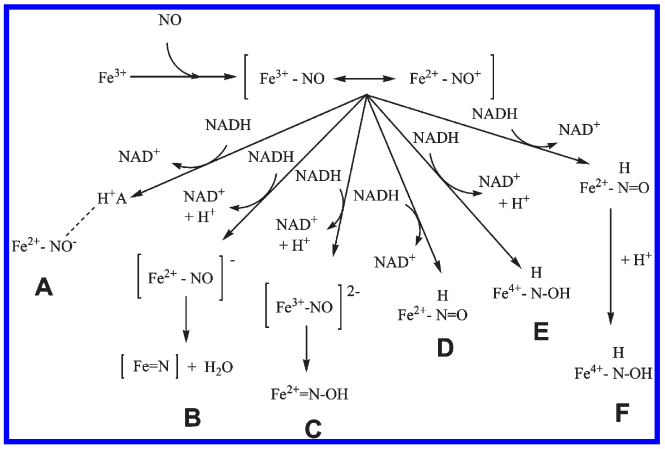

Figure 1. Theories proposed for the formation of intermediate *I* according to Shiro[10] (A), Harris[13] (B), Tsukamoto[14] (C), Averill[16] (D), Daiber[19] (E), and Lehnert (F).[20] In the figure, Fe represents the entire enzyme.

The ferric resting state of the enzyme binds nitric oxide in the first step. The NADH cofactor reduces this complex to intermediate *I* which reacts with a second molecule of nitric oxide to form the N_2O product. In Figure 1 the theories proposed for the mechanism of formation and the structure of the intermediate *I* have been collected.

The proposed mechanisms can be classified upon the role of NADH. In models A−C, NADH is considered an electron donor, and in models D−F direct hydride shift occurs from NADH to the NO-bound heme complex.

Mechanism A was suggested by Shiro et al. based on kinetic measurements[9] and resonance Raman spectroscopy results.[10−12] NADH reduces the ferric heme-nitrosyl complex with two electrons and forms a ferrous heme-nitroxyl complex stabilized by hydrogen-bonding. As no sign of exchangeable proton connected to nitric oxide was observed in the spectrum, they excluded the possibility of direct hydride transfer. The determined rate constant for the formation of intermediate *I* was measured to be $0.9 \times 10^6\ M^{-1}\ s^{-1}$, in accordance with the known fast reaction catalyzed by $P450_{nor}$.[9] Semiempirical calculations have also been used to study the reaction mechanism (pathways B[13] and C[14]). Pathway B contains an N-ferryl intermediate analogous to oxyferryls of other P450 enzymes.[13] According to pathway C, NADH reduces the ferric heme-nitrosyl complex with two electrons, followed by the protonation of the complex on the oxygen atom.[14] Based on HF and density functional theory (DFT) calculations, Tsukamoto et al. suggested that NADH could reduce the nitric oxide bound iron(III)−porphyrin complex with one electron, followed by the dissociation of NOH ligand from the heme group and forming an NAD(NOH) complex.[15]

Direct hydride transfer mechanism (D) was proposed by Averill leading to an Fe−NHO complex.[16] Vincent et al. studied the entire catalytic cycle with DFT methods mainly focusing on the mechanism of N−N bond formation.[17] Their DFT calculations and kinetic isotope effect (KIE) measurements by Daiber et al. suggested the formation of a doubly protonated intermediate (pathway E).[18,19] DFT calculations by Lehnert et al. gave more detail to this theory by showing that the first step is probably direct hydride transfer from NADH to the nitrogen end of heme-bound nitric oxide, followed by the uptake of a proton from the surrounding environment forming the doubly protonated intermediate *I* (pathway F).[20] Even more straightforward evidence for a direct hydride shift mechanism was the determination of the crystal structure of $P450_{nor}$ in complex with an NADH-analogue, demonstrating that NADH most probably binds to the spacious channel perpendicular to the heme plane, positioning the cofactor in close proximity of the heme.[21] It was also shown, in a theoretical study, that simultaneous accommodation of the NO ligand and the NADH cofactor by $P450_{nor}$ is easily accomplished.[22]

Calculations on $P450_{nor}$ published so far were limited to gas phase calculations using semiempirical or density functional methods. In many cases, DFT calculations can give reliable results on the structure, relative energies, and properties of molecules, and can be used to study the mechanism of reactions.[23] DFT methods, especially with the B3LYP functional, have so far been the method of choice for the study of model systems of P450 enzymes,[24] e.g., the electronic structure of Compound I, the active species of most P450s,[25] reaction mechanisms of hydrogen abstraction, arene[26,27] and alkane hydroxylation, olefin oxidation,[28] and the role of water molecules in P450 enzyme activity.[29] Quantum mechanics (QM) calculations have appeared on predicting the regio- and stereospecificity of P450s. In some cases, these studies were able to locate the place of metabolism of common substrates,[30] but in most cases, it is essential to take into account the protein environment,[31] to obtain product ratios in accordance with the experimental results.[32] Combined quantum mechanics/molecular mechanics (QM/MM) calculations on P450 enzymes have emerged recently and addressed various aspects of P450 chemistry,[33] including the hydroxylation of camphor catalyzed by $P450_{cam}$,[29,34−36] the mechanism of benzene hydroxylation,[37] the effect of external electric field on the catalytic cycle of $P450_{cam}$,[38] the electronic structure of Compound I of various P450 isoforms,[39] and dextromethorphan metabolism by P450 2D6.[32]

According to our best knowledge, so far no QM/MM calculations have been published on the $P450_{nor}$ enzyme, although the results of another study have been recently submitted for publication.[40] The aim of the present study is to investigate in detail the mechanism and stereochemistry of the experimentally favored direct hydride transfer from NADH to the NO-bound heme complex. We use traditional DFT calculations as well as hybrid QM/MM calculations, and study the effect of including the protein environment in the calculations. In most cases, QM/MM studies are based on structures where either small model compounds,[37] or real substrates[32] are docked into the active site of the enzyme, for the lack of substrate−enzyme cocrystallized X-ray structures. Docking methods may or may not take into account the flexibility of protein side-chains surrounding the active site cavity;[41] however, these approaches usually cannot take into account the possible conformation changes of the protein that may occur on substrate binding, which could affect the outcome of computational studies. Various crystal structures of $P450_{nor}$ have been published, including its ferric (Fe^{3+}-containing) resting state,[42] and its adducts with CO[42] or NO.[43] These structures showed that coordination of diatomic ligands causes little perturbation of the original protein conformation. However, when $P450_{nor}$ was cocrystallized with a substrate analogue of NADH (nicotinic acid adenine dinucleotide (NAAD) containing a carboxylic group instead of an amide group), a major conformational change of the protein was observed upon ligand binding.[21] Therefore, in this study we examine the effect of protein conformations upon the mechanism of hydride transfer by comparing QM/MM results on two tertiary complex (enzyme/NO/NADH)

dx.doi.org/10.1021/jp2080918 |*J. Phys. Chem. B* 2012, 116, 872–885

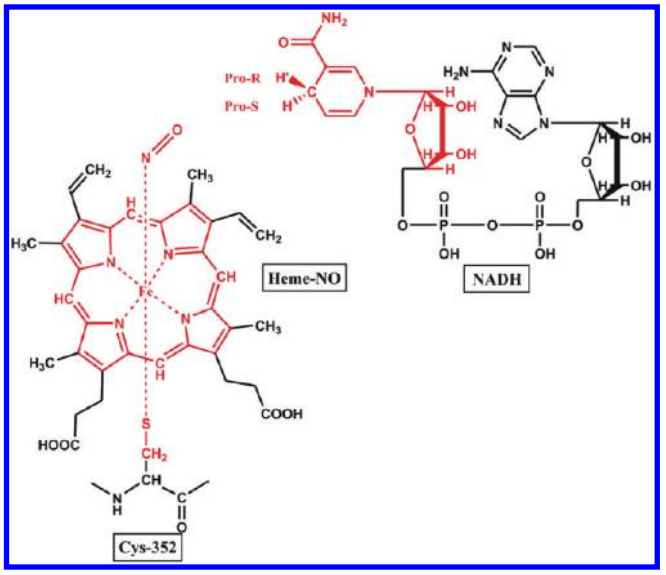

Figure 2. Schematic representation of the system studied in QM-only calculations and of the QM-region of QM/MM calculations (atoms shown in red). On the left side is the complex of the heme and nitric oxide, in which the iron(III) is coordinated to the sulfur of Cys-352 residue. On the right side, NADH is shown with the transferable hydrogens and their spatial position. The split valences of QM region atoms were satisfied by hydrogen atoms in QM-only calculations and by hydrogen-type link atoms in the QM/MM calculations.

models. One was derived previously by one of us[22] from the crystal structure of the NO complex of the enzyme[43] with subsequent docking of the cofactor,[22] while the other was derived from the cofactor-analogue−enzyme complex structure[21] by inserting the NO ligand at the heme site. These two models are of different stereochemistry: in the first, NADH is in an *anti* conformation offering its Pro-S side to the heme and the NO ligand, while the latter is a *syn*-complex, precursor of a Pro-R hydride transfer. The *anti* and *syn* conformations of NADH are distinguished upon the relative orientation of the nicotinamide glycosidic bond with respect to the amide bond.

2. COMPUTATIONAL DETAILS

2.1. QM Calculations. We carried out QM calculations on model systems of the $P450_{nor}$ enzyme. Instead of the protoporphyrin IX ring present in the enzyme, unsubstituted porphine has been used, as it was earlier shown to be a good model of it.[39] The axial cysteine moiety was modeled as a SH^- group, and NAD^+ and NADH were truncated to the nicotinamide moiety with the sugar molecule directly bonded to it (see the red atoms in Figure 2). The same model of NADH has been used successfully to model a hydride transfer reaction in the dihydrofolate reductase enzyme.[44] The calculations were carried out with the Gaussian 09 program package.[45] In order to test the performance of various functionals, we used the pure generalized gradient approximation (GGA) functionals BP86 and OPBE, and the hybrid B3LYP and B3PW91 functionals. These calculations were carried out with the 6-31G(d) basis set on all atoms, except on iron, on which the LANL2DZ pseudo potential was used in conjunction with the corresponding basis set. This basis set composition will be called BS1. To test the effect of the basis set size, the structures were also optimized with the larger cc-pVTZ basis set on all atoms including Fe and the B3LYP functional. Second derivative calculations have been carried out to verify the identity of all located stationary points (using all functionals and BSI), and transition structures were characterized by a single imaginary frequency and minima by only positive frequencies.

Six coordinate ferric NO−heme−thiolate complexes were shown to be EPR silent.[46] The short binding distance of Fe−NO[17] and the characteristically neutral ν_{NO} frequencies measured in the $P450_{nor}$-NO complex[43] all suggest that the spin state of the starting complex of the reaction is a singlet. Therefore, calculations were carried out in this form. Recently, an open-shell singlet state has also been reported for the NO adduct of a heme,[47] but as it was shown to be elusive and not present at all geometries. Therefore we checked the stability of the RKS wave function, but optimization of the wave function led to very slight decrease in energy for the QM models of the starting material and of the intermediate *I* species (see Table S1 in the SI), and therefore we used the closed shell formalism throughout this work, as has been done previously.[48]

As the DFT functionals employed in this work poorly describe dispersion effects, dispersion correction for reaction and activation energies were estimated (where indicated) using the DFT-D3 program developed by Grimme and co-workers.[49]

KIEs were estimated at 298 K from the B3LYP/BSI data by a semiclassical model based on the Eyring equation (eq 1), which can be used to estimate the temperature-dependent rate constant k, as a function of the temperature (T), where $\Delta G^{\ddagger}$ is the free energy of activation of the reaction, R is the universal gas constant, k_B is the Boltzmann constant, and h is the Planck constant.

$$k = \frac{k_B T}{h} \times \exp\left(\frac{-\Delta G^{\ddagger}}{RT}\right) \quad (1)$$

On the basis of eq 1, the semiclassical KIE can be calculated as

$$\mathrm{KIE} = \frac{k_H}{k_D} = \exp[(\Delta G_D^{\ddagger} - \Delta G_H^{\ddagger})/RT] \quad (2)$$

We also estimated the effect of tunneling on the KIE values using Wigner's correction:[50]

$$Q_T = 1 + \frac{u_t^2}{24} \quad (3)$$

and

$$u_t = \frac{h\nu}{k_B T} \quad (4)$$

where ν is the value of the imaginary frequency in the transition state (TS).

These methods have been successfully used to calculate KIE values for hydrogen abstraction reactions catalyzed by other P450 enzymes.[51,52]

2.2. System Setup: MM and Molecular Dynamics (MD) Simulations. Two crystal structures have been used for the QM/MM calculations. Structure **A**, the *anti* complex, was based on the NO-bound crystal structure of $P450_{nor}$ (pdb code: 1CL6[43]) into which NADH has been docked by one of us.[22] Structure **B**, the *syn* complex, was taken from the protein databank (pdb code: 1XQD[21]). This structure contained two mutations (Ser73Gly and Ser75Gly), which were changed back to their original serine residues. Furthermore, the NAAD ligand present in the active site was changed into NADH at the beginning of system setup,

and the NO ligand was added to the structure in a similar position as found in structure **A**. Then, hydrogen atoms were added to the initial enzyme/substrate complexes, and their positions were optimized. Histidine protonation states were assigned according to the model proposed by Menyhárd et al.[22] The protein was truncated to a 25 Å sphere centered on the heme iron. Charged residues at the surface were neutralized to avoid unrealistic effects due to protein truncation and insufficient screening of charges by solvent. For glutamate, aspartate, lysine, and arginine residues near the surface, neutral "patch" residues, with the same geometry but modified atomic charges, were used. The structures were solvated within a 30 Å box with 8000 pre-equilibrated water molecules, represented by the TIP3P model, centered on the heme iron. The added water was then equilibrated by stochastic boundary MD at 300 K over 20 ps with respect to the substrate-bound enzyme structure and minimized. Water molecules more than 25 Å from the heme iron were removed. Then, all atoms were minimized, followed by stochastic boundary MD simulation of the whole system. All systems were heated to 300 K over 60 ps. Subsequent MD equilibrations at 300 K were carried out over 1000 ps. Details of the topology file of the NO-bound heme complex and nonstandard parameters can be found in the Supporting Information (SI). All modeling calculations were carried out using the CHARMM27 force field[53] and the CHARMM software package.[54]

2.3. QM/MM Simulations. The trajectory file of the MD simulation was thoroughly investigated, and several starting structures were selected from the trajectory file of the MD simulation for the QM/MM calculations that could possibly provide a good initial complex for the hydride transfer to occur. Similarly to previous works,[28,32] the initial structures were selected based on geometrical criteria, and structures with short OH and NH distances (between the Fe−NO species and the NADH transferable hydrogen) were chosen. However, in the course of QM/MM calculations, we observed that the NO ligand can rotate around the Fe−N(O) axis relatively freely, and that this rotation did not influence the obtained barriers.

The system was divided into two parts in the QM/MM calculations. The QM-region contained 64 atoms and 10 hydrogen-type link atoms, and it was very similar to the system studied in the QM-only calculations. It included the porphine ring, the NO fragment, the axial cysteine group (Cys-352) modeled as SCH_3^-, and the NADH molecule truncated to the nicotinamide moiety with the sugar molecule directly attached to it (see Figure 2). This selection of QM atoms ensured that only nonpolar C−C bond were cut with no strongly polar groups attached to them. The charges of MM atoms (and the groups they belong to) bonded to QM atoms were set to zero to avoid unphysical effects due to the strong polarization of the QM wave function due to the proximity of large point charges. The MM region consisted of 6046 and 6162 atoms in the case of structures **A** and **B**, respectively. The position of the atoms being farther than 20 Å from the iron atom were fixed in the QM/MM optimizations.

Energy and force calculations on the QM region were carried out with the Gaussian 09 software package at the B3LYP/BS1 level of theory. The MM-region was modeled by the TINKER program[55,56] and CHARMM27 force field.[53] The QoMMMa program[57] was used to couple the input and output files generated by the Gaussian 09 and TINKER program packages.

The starting structures were first thoroughly MM optimized followed by QM/MM optimization. After this we carried out adiabatic mapping to obtain the energy profiles for hydride transfer to the oxygen or nitrogen atom of nitric oxide. This involved decreasing the H−O and H−N distances step by step for the H→O and H→N hydride transfers respectively, and carrying out constrained QM/MM optimization of the whole system.

Single-point calculations were carried out on the critical points of the energy profiles (reactants, products, and TSs) to investigate the effect of the applied functional (BP86, OPBE, B3PW91) in conjunction with the BS1 basis set, and the effect of basis set size was tested by performing single-point calculations at the B3LYP/cc-pVTZ level of theory. All QM/MM calculations were carried out using a restricted Kohn−Sham formalism.

Similarly to QM-only calculation, the effect of dispersion on the relative energies of critical points of selected pathways (only included in energies where indicated) has been estimated using the DFT-D3 program.[49]

3. RESULTS AND DISCUSSION

First we are going to discuss our results related to the geometry and electronic structure of the starting material (NO complex of ferric heme, [Fe(porph)(SH)(NO)], denoted as **Fe−NO$_{QM}$** and of the products (intermediate *I*) of the hydride transfer reaction. Hydride transfer involving the nitrogen end of **Fe−NO** complexes (denoted H→N), leads to **Fe−NHO$_{QM}$** [Fe(porph)-(SH)(N(H)O)]$^-$, while hydride transfer to the oxygen end of nitric oxide (denoted as H→O) leads to **Fe−NOH$_{QM}$** [Fe(porph)(SH)(NOH)]$^-$.

After discussing the properties of starting and product materials, we will address the mechanism of hydride transfer from NADH to the heme−NO enzyme. In these calculations, our system consisted of a SH-ligated (or SCH_3 in QM/MM calculations) and NO-bound porphine ring with a model of NADH. We obtained reactant complexes (**FeNO$_{QM}$** + NADH), TS and product complexes (**FeNHO$_{QM}$**/**FeNOH$_{QM}$** + NAD^+) using different methodologies/starting structures. We identify these species in the paper by adding a subscript after the name of the species, containing the methodology that we used (**QM** or **QM/MM**), the structure from which it was derived (**A** or **B**), and the hydride transfer pathway to which the species belongs to (**H→O** or **H→N**). For example, **Fe−NO$_{QM,B,H→N}$** refers to the reactant complex obtained in QM-only calculations for the H→N hydride transfer based on structure **B**, **TS$_{QM,A,H→O}$** refers to the QM-only TS located for the hydride transfer reaction to the oxygen of nitric oxide derived upon structure **A**, and **Fe−NOH$_{QM/MM,A,H→O}$** refers to the **Fe−NOH** product complex obtained in the QM/MM calculation of structure **A**.

3.1. Electronic Structure of the Investigated Fe−NO, Fe−NOH, and Fe−NHO complexes. *3.1.1. Starting Material: The Fe−NO Complex.* The **Fe−NO** complex of ferric heme compounds, frequently written as {Fe−NO}^{6} according to the Enemark−Feltham notation, is known to be diamagnetic, and for this reason it has been considered to have a closed-shell singlet ground state. {Fe−NO}^{6}, as the notation shows, contains six electrons in the iron d orbitals and the π^* orbitals of the NO ligand, and is isoelectronic with the CO complexes of ferrous heme compounds. Therefore, it has been argued that {Fe−NO}^{6} has an Fe^{2+}−NO^+ character with almost linear FeNO angle, and that its electronic structure is dominated by very strong back bonding from the metal into the two empty π^* orbitals of NO^+, leading to the net transfer of charge density of one electron from the metal to the ligand.[58] In accordance with this, our QM-only and QM/MM calculations of the starting material show very

dx.doi.org/10.1021/jp2080918 |*J. Phys. Chem. B* 2012, 116, 872–885

Table 1. Mulliken Charges at the B3LYP/BSI Level on Various Atoms and Fragments As Calculated in Reactants, TSs, and Products[a]

species	group charges						
	Fe	N	O	H[b]	NADH[c] (NAD^+)	porphyrin[c]	SH^- (CH_3S^-)[c]
				QM-Only Calculations			
Fe−NO$_{QM}$	0.22	0.19	−0.12			−0.27	−0.03
Fe−NOH$_{QM}$	0.19	−0.10	−0.44	0.44		−0.71	−0.38
Fe−NHO$_{QM}$	0.25	−0.12	−0.32	0.30		−0.76	−0.35
Fe−NO$_{QM,A,H\rightarrow O/H\rightarrow N}$	0.19	0.19	−0.08	0.17	0.03	−0.31	−0.02
TS$_{QM,A,H\rightarrow O}$	0.22	−0.09	−0.33	0.39	0.79	−0.48	−0.11
Fe−NOH$_{QM,A,H\rightarrow O}$	0.21	−0.25	−0.49	0.46	0.79	−0.52	−0.20
TS$_{QM,A,H\rightarrow N}$	0.20	−0.04	−0.21	0.28	0.67	−0.49	−0.12
Fe−NHO$_{QM,A,H\rightarrow N}$	0.20	−0.15	−0.33	0.28	0.76	−0.58	−0.19
Fe−NO$_{QM,B,H\rightarrow O/H\rightarrow N}$	0.20	0.18	−0.09	0.16	0.03	−0.29	−0.02
TS$_{QM,B,H\rightarrow O}$	0.19	0.00	−0.37	0.40	0.81	−0.47	−0.16
Fe−NOH$_{QM,B,H\rightarrow O}$	0.23	−0.23	−0.45	0.45	0.76	−0.56	−0.21
TS$_{QM,B,H\rightarrow N}$	0.18	−0.05	−0.22	0.29	0.67	−0.48	−0.11
Fe−NHO$_{QM,B,H\rightarrow N}$	0.18	−0.14	−0.32	0.33	0.70	−0.57	−0.18
				QM/MM Calculations			
Fe−NO$_{QM/MM,A,H\rightarrow O}$	0.20	0.20	−0.09	0.17	0.00	−0.28	−0.03
	(0.01)	(0.01)	(0.01)	(0.01)	(0.00)	(0.01)	(0.03)
TS$_{QM/MM,A,H\rightarrow O}$	0.22	0.08	−0.26	0.37	0.38	−0.37	−0.05
	(0.02)	(0.04)	(0.02)	(0.02)	(0.09)	(0.04)	(0.04)
Fe−NOH$_{QM/MM,A,H\rightarrow O}$	0.25	−0.09	−0.44	0.45	0.64	−0.54	−0.26
	(0.04)	(0.05)	(0.01)	(0.00)	(0.04)	(0.04)	(0.05)
Fe−NO$_{QM/MM,A,H\rightarrow N}$	0.21	0.19	−0.10	0.16	0.01	−0.28	−0.02
	(0.01)	(0.00)	(0.01)	(0.01)	(0.01)	(0.00)	(0.01)
TS$_{QM/MM,A,H\rightarrow N}$	0.23	−0.01	−0.17	0.25	0.54	−0.46	−0.12
	(0.02)	(0.02)	(0.03)	(0.01)	(0.05)	(0.01)	(0.02)
Fe−NHO$_{QM/MM,A,H\rightarrow N}$	0.24	−0.11	−0.29	0.29	0.59	−0.52	−0.20
	(0.02)	(0.01)	(0.01)	(0.01)	(0.04)	(0.03)	(0.02)
Fe−NO$_{QM/MM,B,H\rightarrow O}$	0.19	0.19	−0.11	0.15	0.00	−0.23	−0.04
	(0.00)	(0.01)	(0.04)	(0.03)	(0.00)	(0.03)	(0.02)
TS$_{QM/MM,B,H\rightarrow O}$	0.21	0.00	−0.32	0.40	0.59	−0.38	−0.11
	(0.01)	(0.07)	(0.01)	(0.01)	(0.15)	(0.04)	(0.05)
Fe−NHO$_{QM/MM,B,H\rightarrow O}$	0.21	−0.14	−0.47	0.45	0.68	−0.49	−0.24
	(0.04)	(0.03)	(0.06)	(0.01)	(0.09)	(0.02)	(0.03)
Fe−NO$_{QM/MM,B,H\rightarrow N}$	0.19	0.19	−0.10	0.13	−0.01	−0.23	−0.04
	(0.00)	(0.01)	(0.02)	(0.01)	(0.01)	(0.03)	(0.02)
TS$_{QM/MM,B,H\rightarrow N}$	0.18	−0.04	−0.21	0.29	0.61	−0.42	−0.12
	(0.01)	(0.02)	(0.02)	(0.00)	(0.04)	(0.05)	(0.01)
Fe−NHO$_{QM/MM,B,H\rightarrow N}$	0.21	−0.13	−0.37	0.32	0.69	−0.53	−0.19
	(0.02)	(0.02)	(0.01)	(0.02)	(0.05)	(0.07)	(0.03)

[a] For QM/MM calculations, charges have been averaged over the corresponding profiles and are given with their standard deviation. [b] Hydrogen that is transferred in the form of hydride. [c] Sum of partial atomic charges over the atoms of the fragment.

small charge on both atoms of NO (see Table 1.). This effect we observed with all DFT functionals and basis sets. (Table S2 in the SI)

Another feature of **Fe−NO** complexes is the very short Fe−N(O) bond length. In the crystal structure of structure **A** (complex of $P450_{nor}$ with NO), Fe−N bond length of 1.63 Å, and NO bond length of 1.17 Å have been reported.[43] The calculated bond lengths in the QM/MM calculations are about 1.69 Å, thus slightly longer than the value measured in the X-ray structure, but they are very close to the QM-only calculated value **Fe−NO**$_{QM}$. In contrast, the calculated N−O bond lengths are shorter than the X-ray value (1.17 Å), but close to the 1.15 Å calculated at the B3LYP/BSI level of theory. The values calculated with the other functionals show a very similar picture, the OPBE functional giving values closest to the experiment. The calculated Fe−NO angles are also close to the experimental value (161°) for both structures **A** and **B**, as well as in the QM-only calculation.

dx.doi.org/10.1021/jp2080918 |J. Phys. Chem. B 2012, 116, 872–885

Table 2. Selected Bond Lengths in (Å) and NO Vibration Frequency (cm^{-1}) of the $\{FeNO\}^6$ and $\{FeNO\}^8$ Species Studied in the Gas Phase at the B3LYP/BS1 and BP86/BS1 (in Parentheses) Levels of Theory

heme complex	Fe−S	Fe−N	N−O	ν(NO)[a]	free ligand	N−O	ν(NO)
Fe−NO	2.304	1.687	1.149	1958	NO	1.159	1991
	(2.295)	(1.680)	(1.170)	(1866)		(1.173)	(1891)
Fe−NO$^-$	2.833	1.820	1.221	1555	NO$^-$	1.276	1472
	(2.833)	(1.820)	(1.221)	(1523)		(1.292)	(1394)
Fe−NOH	2.456	1.758	1.327	1099	NOH	1.258	1281
	(2.430)	(1.757)	(1.350)	(1008)		(1.252)	(1074)
Fe−NHO	2.404	1.824	1.231	1550	NHO	1.207	1686
	(2.378)	(1.809)	(1.250)	(1465)		(1.219)	(1524)

[a] Experimental value measured in the crystal is 1851 cm^{-1}.[42]

The Fe−S distance shows the largest variation in our QM/MM calculations. Its experimental value is 2.31 Å in structure **A**[43] and 2.51 Å in structure **B**.[21] The calculated values are in the range of 2.34−2.47 Å, but closer to the lower end of the range, thus closer to the value reported for the NO-bound crystal.

The measured vibrational frequency of the NO stretch is 1851 cm^{-1} in the crystal,[43] and in **Fe−NO$_{QM}$** we calculated 1958 cm^{-1} with the B3LYP and 1886 cm^{-1} with the BP86 functional (Table 2). Similarly, the calculated vibrational frequency of the NO radical is 1991 cm^{-1} with the B3LYP and 1891 cm^{-1} with the BP86 functional versus the experimental 1904 cm^{-1}.[59] The same situation is found for **Fe−NHO$_{QM}$** and **Fe−NOH$_{QM}$**: the BP86 frequencies are lower by about 100 cm^{-1} than the B3LYP values. These results give additional support to the recent findings that GGA functionals, especially the BP86 functional, give accurate vibrational frequencies for heme-nitrosyls, while the B3LYP values are too high by about 100 cm^{-1}.[60]

3.1.2. Intermediate I: Fe−NHO$_{QM}$ and Fe−NOH$_{QM}$ Complexes. These two complexes, **Fe−NHO$_{QM}$** and **Fe−NOH$_{QM}$**, can be considered protonated forms of an $\{Fe{-}NO\}^8$ complex, and for comparison we also investigated the nonprotonated form of the $\{Fe{-}NO\}^8$ complex. All three complexes contain eight electrons in the iron d orbitals and the ligand π^* orbitals. Formally, they could be considered $Fe^{1+}{-}NO$ or $Fe^{2+}{-}NO^-$ species. In the case of a model five-coordinate heme compound, $[Fe(porphine)NO)]^-$, Pellegrino et al. argued that its electronic structure is intermediate between these two limiting scenarios.[61] Analysis of the charges on the different atoms of these complexes show a similar scenario for these $\{Fe{-}NO\}^8$ complexes, as the two extra electrons in these complexes, compared to Fe−NO, are spread over the NO, porphyrin, and SH (SCH_3 in QM/MM) ligands, while the charge on iron remains similar to that of the Fe−NO complexes in both QM/MM and QM-only calculations. An interesting difference between the **Fe−NHO** and **Fe−NOH** complexes is that, when hydrogen is bonded to the nitrogen of nitric oxide, it bears a much smaller charge than in the case of the oxygen protonated form, resulting in a very similar charge on the H−NO fragment in both intermediates and similar overall charges on the other fragments. Molecular orbitals of the protonated $\{Fe{-}NO\}^8$ also reveal their overall similarity, although some difference from the unprotonated $\{Fe{-}NO\}^8$ can be found (see Table S3 in the SI, where we collected the contribution of the various fragments to selected molecular orbitals). In Figure 3 we depicted the molecular orbitals of the **Fe−NHO$_{QM}$** species that show the interaction between NHO, Fe−porphyrin, and SH fragments. The highest occupied molecular orbital (HOMO) of the unprotonated $\{Fe{-}NO\}^8$ corresponds to the interaction between the NO, Fe, and SH fragments, but uptake of the proton significantly decreases the energy of this orbital, and as a consequence it becomes HOMO-7 in the protonated complexes. At the same time, the originally HOMO-1 orbital of the $\{Fe{-}NO\}^8$ complex becomes the HOMO orbital of the protonated $\{Fe{-}NO\}^8$ complexes. This orbital shows bonding contribution between the HNO and Fe fragments, but is strongly antibonding with the sulfur lone pair. An effect of this is the elongated Fe−S distance compared to the **Fe−NO$_{QM}$** species. The Fe−S distance is 2.30 Å in **Fe−NO$_{QM}$**, versus 2.40 Å in **Fe−NHO$_{QM}$** and 2.46 Å in **Fe−NOH$_{QM}$** (see Table 2). Formally, one would expect +1 charge on NAD^+ in product complexes of the QM-only calculations, but interaction with the heme complex induces charge transfer (0.24/0.3 e in the **Fe−NHO$_{QM,A/B,H\rightarrow N}$** product complex and 0.21/0.24 e in the **Fe−NOH$_{QM,A/B,H\rightarrow O}$** product complex; see Table 1) from the **Fe−NHO$_{QM}$** or **Fe−NOH$_{QM}$** species to the NAD^+ molecules. This results in the strengthening and shortening of the Fe−S bond. (Compare data in Tables 2 and 3.)

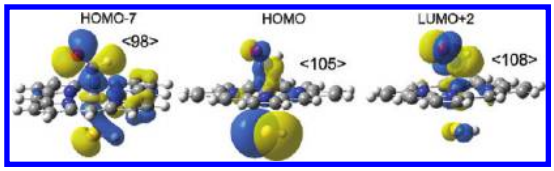

Figure 3. Selected molecular orbitals of the **Fe−NHO$_{QM}$** compound showing the interaction of the NHO, Fe−porphyrin, and SH fragments.

The **Fe−NHO$_{QM}$** and **Fe−NOH$_{QM}$** species with an axial SCH_3 ligand were previously studied by Lehnert et al. using the BP86 functional and an all electron basis set.[20] Comparison of their and our results show that the axial ligand (SH and SCH_3) exerts a similar effect on the properties of these species, and it seems to be independent of the used functional/basis set combination; very similar geometrical parameters and molecular orbitals were obtained in the two studies.

We compared the NO vibrational frequencies in the studied complexes and in the free NO/NOH/NHO/NO^- ligands. In the case of nitric oxide radical, the NO bond length and vibrational frequency is similar in the free and heme bound ligand in accordance with the experimental results,[43,46] while in the case of HNO and NOH, bonding to the ferric heme results in weakening of the NO bond as shown by the elongation of the NO bond length and decreasing vibrational frequency. This effect is even more pronounced for the NOH ligand.

The proton affinity of the N site (of bound NO) of $\{Fe{-}NO\}^8$ is 431 kcal/mol versus 409 kcal/mol of the O site in our calculations, which makes the N-protonated species more stable by 22 kcal/mol in the gas phase, and may suggest a more likely protonation on the N-site in the enzyme as well. This result is in agreement with earlier calculations that reported energy differences of 23 kcal/mol[62] and 26 kcal/mol.[19] This large gas phase proton affinity shows the large basicity of the $\{Fe{-}NO\}^8$ species in accordance with the calculations of Lehnert et al.[20,58] Here we note that the difference between the proton affinities of nitrogen and oxygen sites of the NO^- ligand is even more pronounced: 412 versus 372 kcal/mol at the B3LYP/BSI level, respectively. One of the contributing factors to the smaller difference in the

dx.doi.org/10.1021/jp2080918 |J. Phys. Chem. B 2012, 116, 872–885

Table 3. The Most Important Calculated Geometrical Parameters (at the B3LYP/BSI level, Bonds in Å, Angles in Degrees) for the H→O and H→N Direct Hydride Transfer for Reactant, Tranistion State, and Product Complexes[a]

	Geometrical parameters								
Species	C−H	O−H (N−H)	Fe−N	Fe−S	N−O	NOH (ONH)	CHO (CHN)	FeNO	ΔE
1CL6[43] (1XQD[21])	-	-	1.63	2.31 (2.51)	1.17			161	
QM-Only Calculations									
$Fe-NO_{QM,A,H\rightarrow O}$[b]	1.102	3.919	1.701	2.297	1.145	67	124	156	0.0/0.0/0.0
$TS_{QM,A,H\rightarrow O}$[b]	1.588	1.113	1.784	2.327	1.259	108	158	129	36.1/33.2/29.7
$Fe-NOH_{QM,A,H\rightarrow O}$[b]	4.973	0.994	1.757	2.375	1.360	105	39	119	12.4/12.7/8.6
$Fe-NO_{QM,A,H\rightarrow N}$[b]	1.102	3.619	1.701	2.297	1.145	97	130	156	0.0/0.0/0.0
$TS_{QM,A,H\rightarrow N}$[b]	1.421	1.262	1.805	2.333	1.194	109	152	137	19.5/16.3/11.0
$Fe-NHO_{QM,A,H\rightarrow N}$[b]	2.849	1.051	1.808	2.343	1.244	112	97	134	7.0/6.5/1.4
$Fe-NO_{QM,B,H\rightarrow O}$[b]	1.105	3.276	1.698	2.298	1.147	68	114	157	0.1/-0.4/-1.8
$TS_{QM,B,H\rightarrow O}$[b]	1.609	1.115	1.752	2.359	1.251	119	148	137	40.5/36.8/29.9
$Fe-NOH_{QM,B,H\rightarrow O}$[b]	4.006	0.994	1.760	2.376	1.337	105	36	121	19.0/18.5/11.1
$Fe-NO_{QM,B,H\rightarrow N}$[b]	1.105	3.041	1.698	2.298	1.147	91	131	157	0.1/-0.4/-1.8
$TS_{QM,B,H\rightarrow N}$[b]	1.371	1.278	1.799	2.313	1.193	108	157	142	11.7/8.9/1.7
$Fe-NHO_{QM,B,H\rightarrow N}$[b]	1.992	1.060	1.814	2.340	1.232	112	149	139	7.4/6.7/0.2
QM/MM Calculations									
$Fe-NO_{QM/MM,A}$	1.107	3.370	1.685	2.402	1.146	64	116	160	0.0
$TS_{QM/MM,A,H\rightarrow O}$	1.299	1.176	1.729	2.422	1.192	128	160	154	48.8/46.0/44.7
$Fe-NOH_{QM/MM,A}$	3.098	0.994	1.732	2.567	1.333	106	75	119	45.1/45.3/44.7
$Fe-NO_{QM/MM,A}$	1.103	2.674	1.691	2.453	1.150	90	134	155	0.0
$TS_{QM/MM,A,H\rightarrow N}$	1.507	1.339	1.833	2.548	1.190	108	145	134	31.4/28.2/24.8
$Fe-NHO_{QM/MM,A}$	2.442	1.051	1.804	2.543	1.227	112	133	136	17.4/16.9/15.8
$Fe-NO_{QM/MM,B}$	1.105	2.872	1.677	2.347	1.155	74	127	160	0.0
$TS_{QM/MM,B,H\rightarrow O}$	1.338	1.122	1.740	2.350	1.212	120	173	159	41.7/38.5/38.6
$Fe-NOH_{QM/MM,B}$	3.027	0.992	1.743	2.466	1.365	105	72	118	31.4/30.4/31.4
$Fe-NO_{QM/MM,B}$	1.102	3.739	1.671	2.342	1.143	46	110	169	0.0
$TS_{QM/MM,B,H\rightarrow N}$	1.544	1.248	1.841	2.401	1.192	108	166	132	29.4/27.1/22.4
$Fe-NHO_{QM/MM,B}$	4.240	1.043	1.814	2.433	1.238	111	68	136	20.4/20.3/18.5

[a] Data also shown in Figure 5 for the lowest energy QM TSs. In the case of QM/MM calculations, data is shown for the lowest energy pathways obtained for structures **A** and **B**. Data measured in the X-ray structures are given as a reference. Uncorrected, ZPE-corrected, and ZPE and dispersion corrected relative energies (in this order) are given in kcal/mol at the B3LYP/BS1 level of theory. [b] All energy values are given with respect to $\mathbf{Fe-NO_{QM,A,H\rightarrow O}}$.

case of the porphirin complex is the fact that in $\mathbf{Fe-NOH_{QM}}$ the hydrogen atom is in a bridging position between one of the porphyrin nitrogens and the oxygen ligand, which gives additional stability to the complex (about 6 kcal/mol according to our calculations), compared to the isomer in which the hydrogen is not in bridging position.

3.2. Mechanism of Hydride Transfer from NADH to Fe−NO. *3.2.1. QM-Only Calculations.* We started our QM-only calculations from two structures, which corresponded to the relative orientations of the heme group and NADH observed in structures **A** and **B**. For both orientations, we located the reactant, TS, and product complexes for both H→N and H→O hydride transfer pathways. Results are shown schematically in Figure 4, and the geometrical parameters of these species are collected in Table 3. Relative energies of the different species are given with respect to the energy of the lowest energy van der Waals (or reactant) complex. We used this solution because (1) activation energies compared to van der Waals complexes could be very different from the ones compared to separated fragments,[63] and (2) the reaction results in the formation of charged species (*I* and NAD^+), and it is well-known that in the gas phase separation of oppositely charged ions is strongly endothermic, thus the results would be biased by this effect.

The two located van der Waals complexes have almost identical energies despite their apparently different structure showing negligible interaction (about 0.3 kcal/mol) between the two fragments. At the B3LYP/BS1 level, the van der Waals complex of structure **A** is preferred by 0.1 kcal/mol, but their ordering is reversed using the larger cc-pVTZ basis set (see Table S5/A), or when correction for zero-point energy (ZPE) or for dispersion is taken into account (Table 3).

At the B3LYP/BS1 level, the barriers for hydride transfer are 36.1 kcal/mol (H→O) and 19.5 kcal/mol (H→N) for structure **A**, and 40.4 kcal/mol (H→O) and 11.6 kcal/mol (H→N) for structure **B**. (TS structures ($\mathbf{TS_{QM,B,H\rightarrow O}}$ and $\mathbf{TS_{QM,B,H\rightarrow N}}$) that were derived from structure **B** maintained their original orientation due to the interaction between the amide group of the NADH model and the porphyrin ring. However, in the TSs based on structure **A** ($\mathbf{TS_{QM,A,H\rightarrow O}}$ and $\mathbf{TS_{QM,A,H\rightarrow N}}$), no such interaction was present, and, as a consequence, larger geometrical changes were observed in the orientation of the nicotinamide

dx.doi.org/10.1021/jp2080918 |*J. Phys. Chem. B* 2012, 116, 872–885

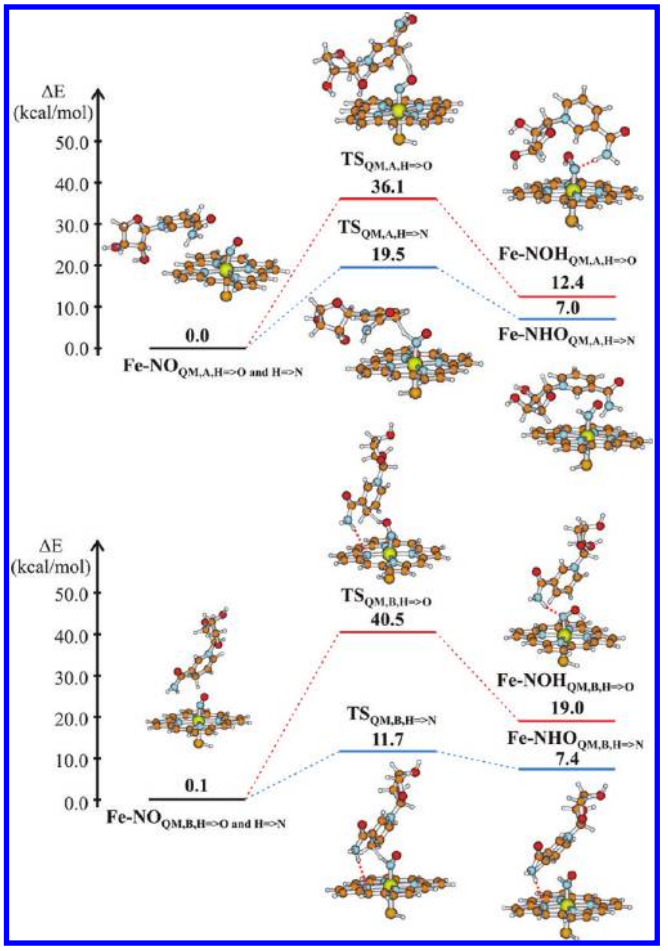

Figure 4. QM-only pathways for H→N (blue) and H→O hydride transfer pathways for heme NADH orientations observed in structures **A** and **B**. All relative energies are given with respect to the energy of the van der Waals complex based on structure **A**.

ring and the attached sugar moiety. The barriers for the H→N hydride transfer reaction are much lower (by about 20 kcal/mol) than those of the H→O hydride transfer reactions. This large energy difference between H→O and H→N TSs seems to resemble the energy difference between the free **FeNOH$_{QM}$** and **FeNHO$_{QM}$** species. Thus our results strongly support the idea of direct hydride transfer from NADH to the N site of the nitric oxide bound the heme-moiety, and the obtained low barrier (11.6 kcal/mol, 9.3 kcal/mol compared to its van der Waals complex when ZPE correction is taken into account) for the model based on the cocrystallized enzyme−substrate analogue complex (**TS$_{QM,B,H→N}$**) is in good agreement with the experimental value of 8.8 kcal/mol for the formation of *I*.[9]

In Figure 5 we show the structure, the most important features, and labeling of atoms of the located lowest energy QM TSs for both types of hydride transfer (data is also shown in Table 3). Geometrical data obtained with a wide range of functionals and also at the B3LYP/cc-pVTZ level are shown in tabulated form in the SI (Table S5). Effects of functional type and basis set size will be discussed after the discussion of the QM and QM/MM results. Here we only note that we did not observe any major difference in the structure of the TSs optimized with the different functionals.

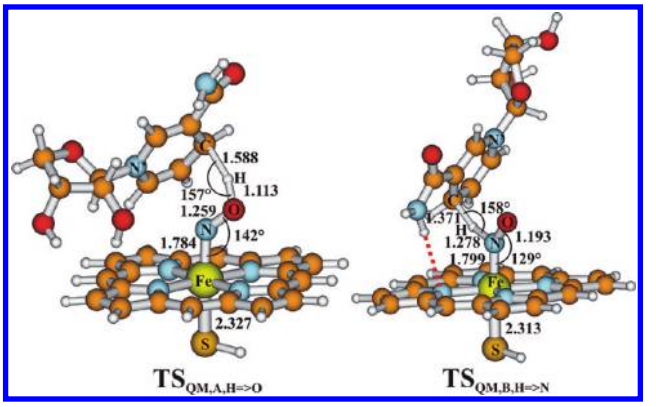

Figure 5. Structure of the lowest energy TSs obtained in QM-only calculations for H→N- and H→O-type hydride transfer reactions. Labels used in tables are also shown.

Despite the large energy differences calculated for the different H→O- and H→N-type TSs, the most important geometrical parameters (Table 3 and Table S5) and charge values (Table 1) show remarkable similarities. All located TSs are relatively late, especially for the H→O reactions. In all TSs, the Fe−N(O) bond is elongated, the FeNO bond angle decreased to their final values, and the Fe−S and N−O bond lengths are intermediate between the reactant and product complexes. The geometry around the hydride is slightly bent with an angle of about 158° in all located TSs. This arrangement is similar to hydride transfer reactions observed in other systems where the angle around the hydride ion was calculated to be in the range of 140−170°.[44,64] One of the differences between the H→O- and H→N-type TSs is the distance of the hydride ion from the nitrogen/oxygen and the carbon atoms. In the H→N TSs, the hydride is in a more intermediate position between the nitrogen and carbon atoms, while in the H→O-type TSs, the H−O bond is almost completely formed. In principle, the emerging aromaticity of the forming nicotinamide ring of NAD^+ could lower the energy of the TS, and, in accordance with this, the sum of the angles around C (the carbon from which the hydride is transferred) is 150° in the H→N and 155° in the H→O TSs. On the basis of electronic reasons, it is expected that it should be easiest to remove the hydride from the nicotinamide ring perpendicularly, and indeed TSs with smaller N−CH angles had lower energies for both type of reactions. Measured N−CH angles are 94° and 107° for the H→O reactions, and 109° and 120° for H→N reactions.

The product complexes are not much higher in energy than the van der Waals complexes, by about 7 kcal/mol for both **Fe−NHO$_{QM,A/B,H→N}$** product complexes and by 12 and 19 kcal/mol in the case of the **Fe−NOH$_{QM,A/B,H→O}$** product complexes. On the basis of this, the O-protonated $\{Fe−NO\}^8$ complexes are only 5 and 12 kcal/mol higher in energy than the N-protonated $\{Fe−NO\}^8$ complexes when the interaction with NAD^+ is also considered. This is remarkable if we take into account that the energy difference between the free **Fe−NHO$_{QM}$** and **Fe−NOH$_{QM}$** complexes is about 20 kcal/mol.

In order to understand why the interaction with NAD^+ stabilizes more **Fe−NOH$_{QM}$** than **Fe−NHO$_{QM}$**, we carried out a few additional calculations on these two systems. We calculated the energy of the NAD^+ and **Fe−NOH$_{QM}$**/**Fe−NHO$_{QM}$** fragments separately at the geometry found in the product complex and calculated (1) the energy difference between **Fe−NOH$_{QM}$**, and **Fe−NHO$_{QM}$** found in **Fe−NOH$_{QM,A/B,H→O}$**

dx.doi.org/10.1021/jp2080918 |*J. Phys. Chem. B* 2012, 116, 872–885

Table 4. Energy Decomposition of the Factors Responsible for Larger Stabilization of the $FeNOH_{QM,H\rightarrow O}$ Complexes with Respect to $FeNHO_{QM,H\rightarrow N}$ Complexes at the B3LYP/BSI Level[a]

	structure **A**	structure **B**
fragment	$E_{A,H\rightarrow O}$-$E_{A,H\rightarrow N}$[c]	$E_{B,H\rightarrow O}$-$E_{B,H\rightarrow N}$[c]
ΔE(**Fe**−**NOH**$_{QM,H\rightarrow O}$ − **Fe**−**NHO**$_{QM,H\rightarrow N}$)	5.4	11.6
ΔE(HEM−NO(H))[b]	22.1 (23.1)	21.0 (22.6)
ΔE(NAD^+)[b]	5.2 (4.5)	0.8 (1.1)
$E_{int,H\rightarrow O}$[d]	−90.7 (−84.5)	−76.9 (−73.5)
$E_{int,H\rightarrow N}$[e]	−68.8 (−62.3)	−66.8 (−61.5)
ΔE_{int}[f]	−21.9 (−22.2)	−10.1 (−12.0)

[a] Data in parentheses refer to calculations with all basis functions of the product complex used in the calculations of the fragments. [b] The fragment was calculated at the same geometry as found in the complex. [c] Difference between the energies of the given fragment in **Fe**−**NOH**$_{QM,H\rightarrow O}$ and **Fe**−**NHO**$_{QM,H\rightarrow N}$. [d] $E_{int,H\rightarrow O} = E$(**Fe**−**NOH**$_{QM,H\rightarrow O}$) − E(HEM−NOH) − E(NAD^+). [e] $E_{int,H\rightarrow N} = E$(**Fe**−**NHO**$_{QM,H\rightarrow N}$) − E(HEM−NHO) − E(NAD^+). [f] $\Delta E_{int} = E_{int,H\rightarrow O} - E_{int,H\rightarrow N}$.

and **Fe**−**NHO**$_{QM,A/B,H\rightarrow N}$, (2) the energy difference arising from the geometry difference of NAD^+ observed in **Fe**−**NOH**$_{QM,A/B,H\rightarrow O}$ and **Fe**−**NHO**$_{QM,A/B,H\rightarrow N}$, (3) the interaction energies between the **Fe**−**NOH**$_{QM}$/**Fe**−**NHO**$_{QM}$ fragment and NAD^+, and (4) the total interaction energy difference between the corresponding **Fe**−**NOH**$_{QM,A/B,H\rightarrow O}$ and **Fe**−**NHO**$_{QM,A/B,H\rightarrow N}$ complexes, i.e., for structures **A** and **B**. The results are shown in Table 4. The energy difference between the heme−NO(H) fragments found in **Fe**−**NOH**$_{QM,A/B,H=>O}$ and **Fe**−**NHO**$_{QM,A/B,H=>N}$ in structure **A** and **B** is 20 kcal/mol, thus it is very similar to the value obtained for the separately optimized fragments. In **Fe**−**NOH**$_{QM,A,H\rightarrow O}$ NAD^+ is in a slightly less advantegous conformation than in **Fe**−**NOH**$_{QM,A,H\rightarrow O}$: its energy is higher by 5 kcal/mol. The energy of NAD^+ is very similar in the product complexes based on structure **B** in accordance with our expectations based on their overall similarity. These observations show that the low energy of the **Fe**−**NOH**$_{QM,A,H\rightarrow O}$ complex and, to a smaller extent, of the **Fe**−**NOH**$_{QM,B,H\rightarrow O}$ is not due to geometric differences but results from the stronger electrostatic interaction between NAD^+ and **Fe**−**NOH**$_{QM}$. In these complexes, there is a hydrogen bond between the nitrogen of the nitric oxide of **Fe**−**NOH**$_{QM,A/B,H\rightarrow O}$ and the amide group of NADH (see also Figure 4). Such a hydrogen bond is not found in the H→N-type product complexes. The difference in the interaction energies between the **Fe**−**NOH**$_{QM,A/B,H\rightarrow O}$ and **Fe**−**NHO**$_{QM,A/B,H\rightarrow N}$ complexes is 22.2 kcal/mol in structure **A** and 12.0 kcal/mol in structure **B**.

The surprisingly large interaction energy between NAD^+ and **Fe**−**NOH** raises the question of whether **Fe**−**NOH**$_{QM,A/B,H\rightarrow O}$ might be formed in the enzyme. The large activation energy for direct hydride transfer to the O of nitric oxide rules out this possibility, but a low energy TS may exist for the isomerization of **Fe**−**NHO**$_{QM,A/B,H\rightarrow N}$, to **Fe**−**NOH**$_{QM,A/B,H\rightarrow O}$, thus the O-protonated form might also be present in small quantities in the enzyme. Due to the shape of the active site of $P450_{nor}$, it is unlikely that **Fe**−**NOH**$_{QM,A,H\rightarrow O}$ could be formed, but the formation of **Fe**−**NOH**$_{QM,B,H\rightarrow O}$ cannot be excluded based on geometrical criteria. However, this state is higher by 12 kcal/mol than the N-protonated form, and using Boltzmann-distribution we predict that this state would probably be present in a very small fraction.

In the case of large systems, dispersion can significantly influence reaction barriers and relative energies. Indeed, for both reactions, dispersion significantly (by about 4 and 6 kcal/mol for the H→O and H→N reactions, respectively) reduces the barrier height and the relative energy of the product (see Table 3).

The calculated KIE based on the semiclassical model (values with Wigner-correction in brackets) ($KIE_{QM,A,H\rightarrow N}$ = 4.46[5.53], $KIE_{QM,B,H\rightarrow N}$ = 4.34[5.17], $KIE_{QM,A,H\rightarrow O}$ = 3.28[3.60], $KIE_{QM,B,H\rightarrow O}$ = 3.81[4.28], for all data see Table S4 in the SI) are in agreement for all TSs with the experimental value of 2.7 ± 0.4.[19] Inclusion of tunneling correction in the KIE calculations slightly increases the obtained KIE values, worsening the agreement with the experiment.

Analysis of the charges on various fragments supports the findings based on geometrical parameters. Formally, at the end of the reaction, the charge on NAD^+ should be +1, and on the heme moiety −1, but the calculated Mulliken charges are slightly lower: showing 0.7−0.8e on NAD^+. Values are slightly larger for the H→O reactions (see Table 1). In the TS of the H→N reaction, the TS is already the largest part of the charge (0.67 e), while in the H→O reactions, all charge (0.79 e) or even more charge (0.81 e) than at the end of the reaction is transferred to the heme−NO moiety. This charge is well spread over all fragments with the exception of Fe, whose charge hardly changes in the course of the reactions. In the H→O reactions, charge reorganization/charge transfer back from NAD^+ occurs after the TS. This charge shows that there is some charge transfer between the Fe−NO(H) and NAD^+ fragments formally at the end of the reaction. We observed the same trends in the case of other functionals and also at the B3LYP/cc-pVTZ level (see Table S2). The major difference between the BS1 and cc-pVTZ results is that, using this larger, all-electron basis set on Fe, the charge on iron increased to about 0.5 e versus the 0.2 e observed with the LANL2DZ pseudopotential, and at the same time, the charge on the porphyrin and SH^- decreased considerably. Charges on other fragments are very similar with the small and large basis sets.

3.2.2. Mechanism of Hydride Transfer from NADH to Fe−NO in QM/MM Calculations. We investigated the possibility of hydride transfer from the NADH to the nitrogen or oxygen of nitric oxide coordinated to the heme iron using two tertiary enzyme models. Before discussing our results, it is worth comparing structures **A** and **B**. Structure **A** is based on the 1CL6 X-ray structure of $P450_{nor}$ in complex with NO[43] into which NADH was docked,[22] while structure **B** is based on the NAAD-bound X-ray structure of $P450_{nor}$[21] in which the NO ligand was missing. The two structures show numerous similarities but also major differences. In both structures, the NADH (or NAAD) cofactor

dx.doi.org/10.1021/jp2080918 |*J. Phys. Chem. B* 2012, 116, 872–885

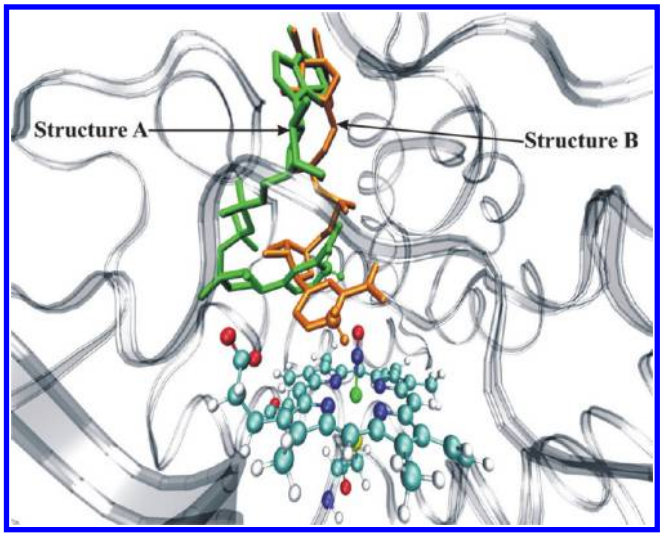

Figure 6. Orientation of NADH with respect to the heme group in structures **A** (green) and **B** (yellow). Transferable hydrogen atoms of NADH are shown in ball-and-stick; the other hydrogen atoms of NADH were omitted for clarity.

is bound in the heme-distal pocket, with the nicotinamide ring reaching over the heme plane and the adenine nucleotide to the solvent (see Figure 6). The binding of NADH in structure **A** and NAAD in structure **B** caused the greatest rearrangement of the B′ helix of $P450_{nor}$ compared to the original ligand free X-ray structure of $P450_{nor}$, and the backbone structure around Arg-174, which is the key interacting residue of the protein matrix of the complex in both structures. However, the two structures differ in the role of Arg-64, which in structure **B** takes part in direct coordination of the cofactor (see Figure 7).[22] As a consequence of these differences, NADH has been differently oriented with respect to the heme in the two structures in our studies as shown in Figure 6.

In principle, there are two hydrogen atoms present in NADH that could be transferred to Fe−NO in the form of hydride ion, but according to KIE on $P450_{nor}$, the transfer of pro-R hydrogen is favored.[19] Due to the different orientation of NADH in the two models considered by us, structure **B** leads to Pro-R, while structure **A** leads to Pro-S stereoselectivity. Usage of two different protein models enables us to computationally investigate the effect of the protein matrix on the reaction mechanism and how it influences the stereoselectivity of the enzyme.

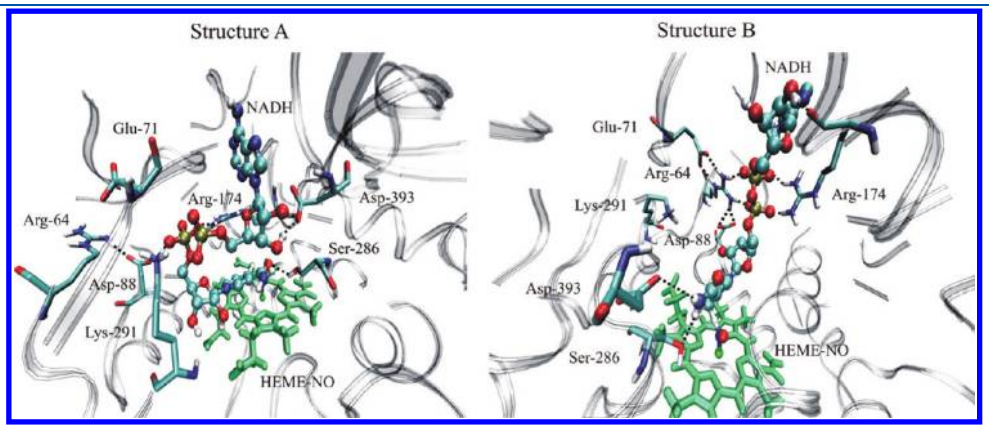

Figure 7. Interaction of NADH with the protein matrix via hydrogen bonds in structures **A** and **B**.

Table 5. Comparison of the Performance of Different Functionals and Basis Sets on the Energetics of Different Profiles Obtained for Structure A and QM-Only Results for Structures Based on Structure A[a]

		B3LYP BS1		B3LYP cc-pVTZ		BP86 BS1		OPBE BS1		B3PW91 BS1	
	profile	ΔE	$\Delta E^{\ddagger}$	ΔE	$\Delta E^{\ddagger}$	ΔE	$\Delta E^{\ddagger}$	ΔE	$\Delta E^{\ddagger}$	ΔE	$\Delta E^{\ddagger}$
QM/MM H→O structure **A**	1	46.1	59.4	48.1	60.6	52.4	53.3	60.4	61.0	50.6	60.7
	2	45.1	48.8	48.3	52.2	50.6	53.1	67.2	61.9	49.7	52.7
	3	39.5	52.4	42.3	52.4	44.9	44.8	52.2	51.1	46.4	53.0
	3[b]	44.3	51.3	47.9	52.7	48.8	43.5	56.8	49.9	48.6	51.9
QM/MM H→N structure **A**	4	28.4	43.5	32.4	47.4	35.9	47.4	43.2	57.3	32.2	47.3
	5	17.4	31.4	21.8	36.4	25.2	30.3	32.5	39.5	20.9	33.4
	6	25.0	34.2	29.2	38.3	31.4	37.8	38.2	46.1	28.4	37.5
	7	26.9	40.6	32.3	46.2	34.4	38.3	43.2	48.4	30.6	42.5
	5[b]	12.2	25.6	16.2	30.1	20.9	24.6	26.7	33.3	15.5	27.3
QM, H→O		12.4	36.1	17.6	39.7	18.3	34.2	34.4	49.4	15.5	36.6
QM, H→N		7.0	19.5	11.1	24.2	12.6	n.c.[c]	24.3	28.5	9.7	20.2

[a] Results of single-point calculations are presented for QM/MM calculations, while QM-only structures were fully optimized with the given methods. All values are given in kcal/mol. [b] These results correspond to single-point calculations on the indicated profiles by deleting point charges from the QM Hamiltonian and removing all interaction with the protein. [c] n.c. = not converged.

dx.doi.org/10.1021/jp2080918 |*J. Phys. Chem. B* 2012, 116, 872–885

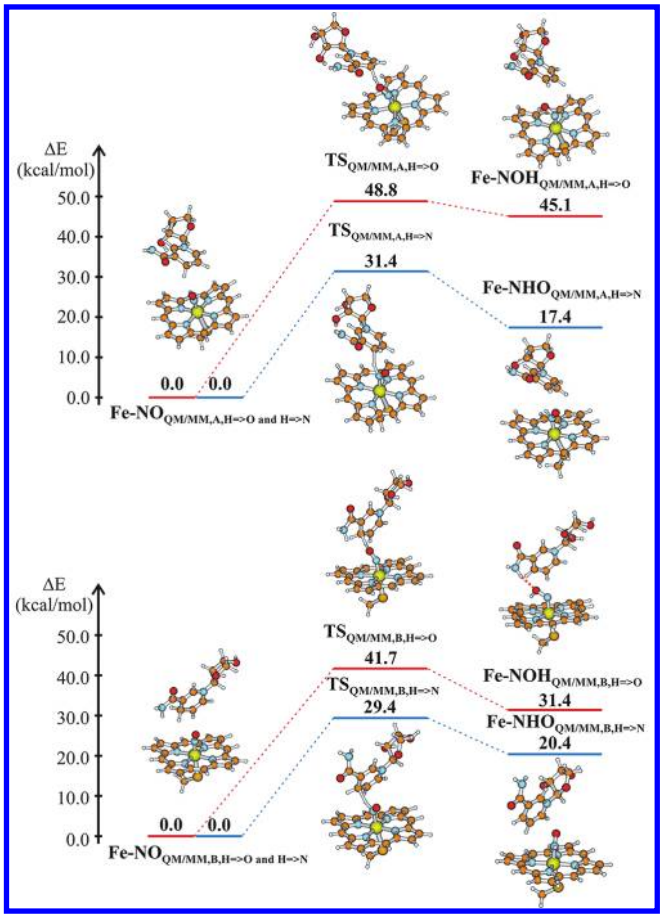

Figure 8. Lowest energy pathways obtained in QM/MM calculations for H→N (blue) and H→O (red) hydride transfer pathways in structures **A** and **B**.

The obtained energy barriers, reaction energies, and geometrical parameters for the lowest energy pathways are given in Table 3 for structures **A** and **B**. Details of all pathways are given in the SI in Table S5. The obtained energy profiles are shown in Figures S1 and S2 in the SI. Results of single-point calculations are shown in Table 5 for structure **A** and the hydrogen bonds between NADH, and the protein matrix observed in the QM/MM TSs of the H→N profiles are shown in Figure 7.

The barriers obtained for the H→N-type hydride transfer in structure **A** are 31.4, 34.2, 40.6, and 43.5 kcal/mol, and in structure **B** they are 29.4, 31.2, and 33.3 kcal/mol. For the H→O-type hydride transfer, the barriers are, in structure **A**, 48.8, 52.4, and 59.4 kcal/mol, and, in structure **B**, 41.7, 45.7, and 48.1 kcal/mol. ZPE-correction (derived upon the corresponding QM-only calculations) reduces the H→N barriers by about 2 kcal/mol, while leaving the H→O barriers practically unchanged. Dispersion correction also has a larger effect on the H→N barriers, and our best estimates of the reaction barriers (including ZPE and dispersion correction) are 44.7 (for H→O) and 24.8 (for H→N) kcal/mol for structure **A** and 38.6 (for H→O) and 22.4 (for H→N) for structure **B**. These barriers are higher than the experimental value (8.8 kcal/mol),[9] but the H→N barrier in structure **B** is similar to the QM/MM barrier obtained for the hydride transfer in the dihydrofolate enzyme (21 kcal/mol vs the experimental value of 13 kcal/mol).[65] Further sampling of additional QM/MM reaction paths, or calculation of a potential of mean force[66] (e.g., by umbrella sampling MD simulations, which are not feasible yet with DFT QM/MM methods for $P450_{nor}$) could lead to slight reduction of the obtained barriers; however, the very large difference between the barriers of H→N and H→O reactions should not change. The barriers obtained in structure **B** are lower and show significantly less variation than in the case of structure **A**. Another major difference between the results of QM-only and QM/MM calculations is the stability of intermediate *I* compared to the reactant species. While we noted for QM-only calculations that the difference was rather small (about 7 kcal/mol for the H→N reaction and 12 kcal/mol for the H→O reaction), in the QM/MM calculation in the various profiles we observed differences of 30−45 kcal/mol for the H→O reaction and about 17−30 kcal/mol for the H→N reaction, which, even in the lowest energy cases, show the destabilization of the product complexes by about 10 kcal/mol compared to the QM-only calculations (Figure 8).

To test the effect of the enzyme environment on the reaction barrier, we performed single-point calculations on the critical points of the lowest energy profiles of structure **A** by removing the point charges from the QM Hamiltonian (Table 5) as well as other energy terms related to the interaction with the MM region. In the case of the H→O-type reaction, polarization of the QM region causes the slight destabilization of the TS and stabilization of the product, while in the case of the H→N-type reaction, the enzyme environment seems to destabilize both the TS and the product by about 5 kcal/mol. Different QM/MM studies on the hydride transfer step on the dihydrofolate reductase enzyme reported either TS stabilization[67] or TS destabilization.[65] However, even in calculations including nuclear quantum effects,[68] the donor−acceptor distance at the TS was found to be around 2.7 Å, quite similarly to those obtained by us.

TS structures show some variations over the various profiles, although their main characteristics remain the same, independent of the conformation of the protein. It seems that at the atomic level the nature of the TS is more influenced by the intrinsic characteristics of hydride transfer than by the conformation of the surrounding protein. One major difference between TS structures in structures **A** and **B** was the N−CH angle, which was about 130−140° for both pathways in structure **A** and around 100−110° in structure **B**, thus much lower in the *syn* structure of enzyme and NADH analogue. This is an important difference; as was discussed above, angles closer to 90° favor hydride transfer, thus the *syn* structure seems to represent a protein structure more favorable for hydride transfer than the docked structure. QM/MM TSs seem to be more concerted than the QM-only TS, shown by shorter CH and longer OH or NH distances. Also, the sum of bond angles around C (from which the hydride is transferred) is lower than in the QM-only calculations. It is around 338° and 345° for structure **A** and 347° and 348° for structure **B** for the H→O and H→N pathways, respectively. Analysis of charge transfer also indicates an earlier TS in QM/MM calculations than in QM-only calculations. For example, in the case of structure **A**, only 0.38 e is transferred from NADH to the heme−NO complex in the TS, while in the QM-only TS, this value was 0.76 e (Table 1). Apart from differences in the TSs, charge distribution of reactant and product complexes is very similar to that of QM-only calculations, and the standard deviation of the data is also low. However, the overall charge on NADH is lower in general in the QM/MM profiles than in the QM calculations, and this

is especially true for structure **A**. In structure **A**, the charge on Fe in the product complexes is slightly higher than in structure **B**, and at the same time, the Fe−S bond is longer by about 0.1 Å in reactants, TSs, and products, due to the slightly longer hydrogen bond distances to the cysteinyl sulfur coordinating to the heme Fe in structure **A**.

3.2.3. Effect of DFT Functionals. In order to test the reliability of our results, we optimized the structure of QM-only TSs, reactants, and products with numerous functionals (pure GGA functionals BP86 and OPBE, and hybrid B3LYP and B3PW91 functionals) and with the cc-pVTZ basis set using the B3LYP method, and carried out single-point calculations with the same functionals and basis sets on the critical points of profiles obtained for structure **A**. In this section, we would like to give an overview of the obtained trends.

In Table 5 we show the obtained energy barriers and relative energies, while the optimized geometries, relative energies (see Table S5), and charges on different fragments obtained with different functionals (Table S2) are collected in the SI. Reoptimization of the structure of TS did not lead to any major changes. As expected, the B3PW91 functional gave essentially the same structure as B3LYP with similar activation and relative energies. Usage of the large all-electron functional (cc-pVTZ) on all atoms hardly changed the geometry of QM-only optimized structures, but gave higher barriers and relative energies by 4−5 kcal/mol for the TS and product complexes. The pure functionals BP86 and OPBE predict very late TS structure (with very short O−H and N−H distances), and the product complexes lie much higher in energy than the hydride functionals. The barriers with the OPBE functional are about 10 kcal/mol higher than with B3LYP.

The trends observed in the case of single-point calculations for the H→O and H→N reactions are slightly different. For the H→N reactions, the large basis set with the B3LYP functional results in systematic increase of ΔE and $\Delta E^{\ddagger}$ values by 4−5 kcal/mol compared to the small basis set calculations, as seen in the case of QM-only calculations, and actually these numbers are very similar to the B3PW91 values. BP86 gives similar barriers as B3LYP but increases the relative energy of the products by about 5 kcal/mol, while in the case of OPBE both barriers and reaction energies are systematically higher by about 10−15 kcal/mol. The results of single-point calculations for the H→O reaction are more controversial, especially for the reaction energies. Results of profile 2 show completely different trends than those of profiles 1 and 3. We believe that this is due to the different product structures predicted by the various functionals, as single-point calculations on the next to last point on the H→O profiles gave consistently lower (by 2−3 kcal per mol below the energy of the TS) relative energies for the final products. Geometries corresponding to the penultimate points of the H→O profiles are characterized by longer O−H distances, close to the BP86 and OPBE preferred O−H distance in the QM-only calculation of final complexes, and for these points the abrupt increase in energy seen with the OPBE functional for profile 2 was not observed. These single-point calculations call attention to the fact that there is some uncertainty about obtaining correct energetics using single-point calculations when equilibrium geometries differ in the case of the different methods.

4. CONCLUSIONS

In this paper we present the first QM/MM-level calculations considering all reaction partners (enzyme, ligand, cofactor) of the unique reductive NO dimerization reaction carried out by $P450_{nor}$. Results are in agreement with a direct hydride transfer taking place between the NADH cofactor and NO, where the hydride is shifted to the N of NO, and correctly predict the observed stereoselectivity of the reaction.

Our QM-only calculations revealed the overall similarity of the studied $\{Fe-NO\}^8$ complexes, and showed that when a proton is taken up by the unprotonated $\{Fe-NO\}^8$ complex, the energy of the HOMO orbital decreases considerably and becomes HOMO-7 in the protonated complexes. QM-only calculations indicate a very strong preference for hydride transfer from NADH to the nitrogen end of nitric oxide bound to the heme group, and the obtained activation energy and KIE values are in agreement with the experimental results. Hydride transfer to the oxygen end of nitric oxide requires very high activation energies and is unlikely to occur.

We performed QM/MM calculations on two protein models containing *syn* and *anti* stereoisomers of NADH. The *anti* model was derived upon docking of NADH into the active site of the NO-bound $P450_{nor}$ enzyme, while the *syn* model was based upon a cocrystallized structure of $P450_{nor}$ and an NADH analogue. The obtained QM/MM barriers in both structures and for both pathways are higher than the QM-only barriers, but the barriers in the *syn* model are lower and show significantly smaller variation than those in the *anti* model, in accordance with the observed stereoselectivity of the enzyme. The fact that the barriers for H→N hydride transfer are significantly lower in both studied enzyme models suggests that most likely in similar enzymes (e.g., in Nor1p) hydride transfer from NADH follows the same mechanism.

Analysis of the geometrical parameters of QM/MM TSs indicated that the *syn*-complex structure facilitates the formation of a favorable TS for hydride transfer more, allowing the hydride to be removed from the nicotinamide ring in an almost perpendicular fashion, while in the *anti* model, larger angles were observed for the hydride transfer, giving higher activation energies. All located TSs can be considered late as the largest part of charge is transferred from NADH to the heme−NO moiety before reaching the TS, and the nicotinamide ring is almost planar in the TS.

Our study clearly shows that hydride from NADH is transferred to the nitrogen end of nitric oxide. However, due to the pK_a value of the formed **Fe−NHO** intermediate,[20,58] and to the presence of a large amount of water and basic/acidic residues in the active site, we postulate that the key intermediate of the $P450_{nor}$ species is doubly protonated, as has been suggested previously.[17−19]

Comparison of our results obtained for the two protein models implies that (1) ligand-free crystal structures may not be properly set up for accommodating the ligand in an orientation giving rise to the experimentally observed regio-/stereoselectivity, especially when large conformation changes of the protein occur upon ligand binding, (2) in the case of docked models, different interactions may stabilize the position of the ligand than in a real enzyme−substrate complex, e.g., as seen for these two $P450_{nor}$ models, which can lead to higher barriers or to a much wider range of barriers, and (3) cocrystallized structures, where the reacting site is close to the reaction center, may serve as a much better starting structure for QM/MM calculations than docked structures. However, cocrystallized structures are frequently unavailable or the ligand is not bound in the active site of the enzyme, but in a farther position, making the usage of docked

structures inevitable. Therefore we suggest that before using a docked structure for QM/MM studies, a thorough investigation of preferable QM-only TSs should be carried out, and the docking method should allow for protein conformational changes to accommodate the favorable TS structure of the reaction.

■ ASSOCIATED CONTENT

Supporting Information. Selected geometrical parameters and fragment charges for QM-only optimized structures using various functionals and basis sets, and details of all reactant, TS, and product complexes obtained in QM/MM calculations. Furthermore, total energies and Cartesian coordinates of all QM-only structures, geometries of QM/MM structures, and MM parameters for the heme−NO complex are also provided in the SI together with tables and figures indicated in the text. This material is available free of charge via the Internet at http://pubs.acs.org.

■ AUTHOR INFORMATION

Corresponding Author
*E-mail: olahjulcsi@gmail.com.

■ ACKNOWLEDGMENT

J.O. acknowledges receipt of an EU Marie Curie Fellowship (Project "Oestrometab"). Financial support for this work on behalf of D.K.M. was provided by an OTKA grant (NK67800), and a European Union Social Fund grant (TÁMOP 4.2.1./B-09/1/KMR-2010-0003). Financial Support from New Széchenyi Plan (Project ID: TÁMOP-4.2.1/B-09/1/KMR-2010-0002) is acknowledged.

■ REFERENCES

(1) Ortiz de Montellano, P. R.; De Voss, J. J. In *Cytochrome P450*, 3rd ed.; Ortiz de Montellano, P. R., Ed.; Kluwer Academic/Plenum Publishers: New York, 2005; pp 183−245.
(2) Paine, M. J. I.; Scrutton, N. S.; Munro, A. W.; Gutierrez, A.; Roberts, G. C. K.; Wolf, C. R. In *Cytochrome P450*, 3rd ed.; Ortiz de Montellano, P. R., Ed.; Kluwer Academic/Plenum Publishers: New York, 2005; pp 115−148.
(3) de Vries, S.; Schröder, I. *Biochem. Soc. Trans.* **2002**, *30*, 662–667.
(4) Richardson, D.; Felgate, H.; Watmough, N.; Thomson, A.; Baggs, E. *Trends Biotechnol.* **2009**, *27*, 388–397.
(5) Wink, D. A.; Hines, H. B.; Cheng, R. Y. S.; Switzer, C. H.; Flores-Santana, W.; Vitek, M. P.; Ridnour, L. A.; Colton, C. A. *J. Leukocyte Biol.* **2011**, *89*, 873–891.
(6) Chao, L. Y.; Rine, J.; Marletta, M. A. *Arch. Biochem. Biophys.* **2008**, *480*, 132–137.
(7) Zhang, L.; Kudo, T.; Takaya, N.; Shoun, H. *J. Biol. Chem.* **2002**, *277*, 33842–33847.
(8) Kudo, T.; Takaya, N.; Park, S.-Y.; Shiro, Y.; Shoun, H. *J. Biol. Chem.* **2001**, *276*, 5020–5026.
(9) Shiro, Y.; Fujii, M.; Iizuka, T.; Adachi, S.; Tsukamoto, K.; Nakahara, K.; Shoun, H. *J. Biol. Chem.* **1995**, *270*, 1617–1623.
(10) Obayashi, E.; Takahashi, S.; Shiro, Y. *J. Am. Chem. Soc.* **1998**, *120*, 12964–12965.
(11) Obayashi, E.; Shimizu, H.; Park, S.-Y.; Nakamura, H.; Takahashi, S.; Shoun, H.; Shiro, Y. *Int. Congr. Ser.* **2002**, *1233*, 59–62.
(12) Shiro, Y. *Riken Rev.* **1999**, *24*, 56–58.
(13) Harris, D. L. *Int. J. Quantum Chem.* **2002**, *288*, 183–200.
(14) Tsukamoto, K.; Nakamura, S.; Shimizu, K. *J. Mol. Struct. (THEOCHEM)* **2003**, *624*, 309–322.
(15) Tsukamoto, K.; Watanabe, T.; Nagashima, U.; Akiyama, Y. *J. Mol. Struct. (THEOCHEM)* **2005**, *732*, 87–98.
(16) Averill, B. A. *Chem. Rev.* **1996**, *96*, 2951–2964.
(17) Vincent, M. A.; Hillier, I. H.; Ge, J. *Chem. Phys. Lett.* **2005**, *407*, 333–336.
(18) Daiber, A.; Shoun, H.; Ullrich, V. *J. Inorg. Biochem.* **2005**, *99*, 185–193.
(19) Daiber, A.; Nauser, T.; Takaya, N.; Kudo, T.; Weber, P.; Hultschig, C.; Shoun, H.; Ullrich, V. *J. Inorg. Biochem.* **2002**, *88*, 343–352.
(20) Lehnert, N.; Praneeth, V. K. K.; Paulat, F. *J. Comput. Chem.* **2006**, *27*, 1338–1351.
(21) Oshima, R.; Fushinobu, S.; Su, F.; Zhang, L.; Takaya, N.; Shoun, H. *J. Mol. Biol.* **2004**, *342*, 207–217.
(22) Menyhárd, D. K.; Keserű, Gy. M. *J. Mol. Graphics Modell.* **2006**, *25*, 363–372.
(23) Sousa, S. F.; Fernandes, P. A; Ramos, M. J. *J. Phys. Chem. A* **2007**, *111*, 10439–10452.
(24) Shaik, S.; Kumar, D.; de Visser, S. P.; Altun, A.; Thiel, W. *Chem. Rev.* **2005**, *105*, 2279–2328.
(25) Ogliaro, F.; Cohen, S.; de Visser, S. P.; Shaik, S. *J. Am. Chem. Soc.* **2000**, *122*, 12892–12893.
(26) Bathelt, C. M.; Ridder, L.; Mulholland, A. J.; Harvey, J. N. *Org. Biomol. Chem.* **2004**, *2*, 2998–3005.
(27) Shaik, S.; Milko, P.; Schyman, P.; Usharani, D.; Chen, H. *J. Chem. Theory Comput.* **2011**, *7*, 327–339.
(28) Lonsdale, R.; Harvey, J. N.; Mulholland, A. J. *J. Phys. Chem. B* **2010**, *114*, 1156–1162.
(29) Kumar, D.; Altun, A.; Shaik, S.; Thiel, W. *Farad. Discuss* **2011**, *No. 148*, 373–383.
(30) Olsen, L.; Rydberg, P.; Rod, T. H.; Ryde, U. *J. Med. Chem.* **2006**, *49*, 6489–6499.
(31) Ranaghan, K. E.; Mulholland, A. J. *Int. Rev. Phys. Chem.* **2010**, *29*, 65–133.
(32) Oláh, J.; Mulholland, A. J.; Harvey, J. N. *Proc. Natl. Acad. Sci. U.S.A.* **2011**, *108*, 6050–6055.
(33) Shaik, S.; Cohen, S.; Wang, Y.; Chen, H.; Kumar, D.; Thiel, W. *Chem. Rev.* **2010**, *110*, 949–1017.
(34) Zheng, J. J.; Altun, A.; Thiel, W. *J. Comput. Chem.* **2007**, *28*, 2147–2158.
(35) Altun, A.; Shaik, S.; Thiel, W. *J. Am. Chem. Soc.* **2007**, *129*, 8978–8987.
(36) Altarsha, M.; Benighaus, T.; Kumar, D.; Thiel, W. *J. Am. Chem. Soc.* **2009**, *131*, 4755–4763.
(37) Bathelt, C. M.; Mulholland, A. J.; Harvey, J. N. *J. Phys. Chem. A* **2008**, *112*, 13149–13156.
(38) Lai, W. Z.; Chen, H.; Cho, K. B.; Shaik, S. *J. Phys. Chem. Lett.* **2010**, *1*, 2082–2087.
(39) Bathelt, C. M.; Zurek, J.; Mulholland, A. J.; Harvey, J. N. *J. Am. Chem. Soc.* **2005**, *127*, 12900–12908.
(40) Riplinger, C.; Neese, F. *Book of Abstracts*, 3rd Quantum Bioinorganic Chemistry Conference (QBIC-3), Cesky Krumlov, Chech Republic, June 25−28, 2011.
(41) Sotriffer, C. A. *Curr. Top. Med. Chem.* **2011**, *11*, 179–191.
(42) Park, S. Y.; Shimizu, H.; Adachi, S.; Nakagawa, A.; Tanaka, I.; Nakahara, K.; Shoun, H.; Obayashi, E.; Nakamura, H.; lizuka, T.; et al. *Nat. Struct. Biol.* **1997**, *4*, 827–832.
(43) Shimizu, H.; Obayashi, E.; Gomi, Y.; Arakawa, H.; Park, S. Y.; Nakamura, H.; Adachi, S.; Shoun, H.; Shiro, Y. *J. Biol. Chem.* **2000**, *275*, 4816–4826.
(44) Castillo, R.; Andres, J.; Moliner, V. *J. Am. Chem. Soc.* **1999**, *121*, 12140–12147.
(45) Frisch, M. J.; Trucks, G. W.; Schlegel, H. B.; Scuseria, G. E.; Robb, M. A.; Cheeseman, J. R.; Scalmani, G.; Barone, V.; Mennucci, B.; Petersson, G. A. et al. *Gaussian 09*, revision A.1; Gaussian, Inc.: Wallingford, CT, 2009.
(46) Suzuki, N.; Higuchi, T.; Urano, Y.; Kikuchi, K.; Uchida, T.; Mukai, M.; Kitagawa, T.; Nagano, T. *J. Am. Chem. Soc.* **2000**, *122*, 12059–12060.

(47) Praneeth, V. K. K.; Paulat, F.; Berto, T. C.; DeBeer George, S.; Nather, C.; Sulok, C. D.; Lehnert, N. *J. Am. Chem. Soc.* **2008**, *130*, 15288–15303.
(48) Oláh, J.; Harvey, J. N. *J. Phys. Chem. A* **2009**, *113*, 7338–7345.
(49) Grimme, S.; Antony, J.; Ehrlich, S.; Krieg, H. J. *Chem. Phys.* **2010**, *132*, 154104.
(50) Melander, L.; Saunders, W. H., Jr. *In Reaction Rates of Isotopic Molecules; Robert E.*; Krieger Publishing Company: Malabar, FL, 1987.
(51) de Visser, S. P.; Ogliaro, F.; Sharma, P. K.; Shaik, S. *J. Am. Chem. Soc.* **2002**, *124*, 11809–11826.
(52) Li, C.; Wu, W.; Cho, K.-B.; Shaik, S. *Chem.—Eur. J.* **2009**, *15*, 8492–8503.
(53) MacKerell, A. D, Jr.; Banavali, N.; Foloppe, N. *Biopolymers* **2000**, *56*, 257–265.
(54) Brooks, B. R.; Brooks, C. L., III; Mackerell, A. D.; Nilsson, L.; Petrella, R. J.; Roux, B.; Won, Y.; Archontis, G.; Bartels, C.; Boresch, S.; et al. *J. Comput. Chem.* **2009**, *30*, 1545–1615.
(55) TINKER − Home Page. Tinker - Software tools for molecular design. http://dasher.wustl.edu/tinker/ (accessed October 5, 2011).
(56) Ren, P.; Wu, C.; Ponder, J. W. *J. Chem. Theory Comput.* **2011**, *7*, 3143–3161.
(57) Harvey, J. N. *Faraday Discuss.* **2004**, *No. 127*, 165–177.
(58) Goodrich, L. E.; Paulat, F.; Praneeth, V. K. K.; Lehnert, N. *Inorg. Chem.* **2010**, *49*, 6293–6316.
(59) Huber, K. P.; Herzberg, G. *Molecular Spectra and Molecular Structures IV. Constants of Diatomic Molecules*; Van Nostrand Reinhold: New York, 1979.
(60) Brothers, S. M.; Darensbourg, M. Y.; Hall, M. B. *Inorg. Chem.* **2011**, *50*, 8532–8540.
(61) Pellegrino, J.; Bari, S. E.; Bikiel, D. E.; Doctorovich, F. *J. Am. Chem. Soc.* **2010**, *132*, 989–995.
(62) Silaghi-Dumitrescu, R. *Eur. J. Inorg. Chem.* **2003**, *No. 6*, 1048–1052.
(63) Lonsdale, R.; Harvey, J. N.; Mulholland, A. J. *J. Phys. Chem. Lett.* **2010**, *1*, 3232–3237.
(64) Andrés, J.; Molinera, V.; Safont, V. S.; Aulló, J. M.; Díaz, W.; Tapiac, O. *J. Mol. Struct. (THEOCHEM)* **1996**, *371*, 299–312.
(65) Cummins, P. L.; Rostov, I. V.; Gready, J. E. *J. Chem. Theory Comput.* **2007**, *3*, 1203–1211.
(66) Sharma, P. K.; Chu, Z. T.; Olsson, M. H. M.; Warshel, A. *Proc. Natl. Acad. Sci. U.S.A.* **2007**, *104*, 9661–9666.
(67) Garcia-Viloca, M.; Truhlar, D. G.; Gao, J. *J. Mol. Biol.* **2003**, *327*, 549–560.
(68) Hammes-Schiffer, S.; Watney, J. B. *Philos. Trans. R. Soc., B* **2006**, *361*, 1365–1373.